Simplified material assignment for CBCT-based dose calculations of prostate radiotherapy with hip prostheses

Turki Almatani[1,*], Richard P. Hugtenburg[1,2], Ryan Lewis[2], Susan Barley[3], and Mark Edwards[2]

[1] *College of Medicine, Swansea University, Singleton Park , Swansea SA2 8PP, UK*
[2] *Department of Medical Physics and Clinical Engineering, Singleton Hospital, ABM University Health Board, Swansea SA2 8QA, UK*
[3] *Oncology Systems Limited, 14 Longbow Close, Shrewsbury SY1 3GZ, UK*

[*]Corresponding author. E-mail address: turkialmatani@gmail.com (T. Almatani)

Acknowledgement: The authors gratefully acknowledge the staff of the Department of Medical Physics and Clinical Engineering, ABMU for their assistance in this study. The Ministry of Higher Education of Saudi Arabia provided sponsorship for Turki Almatani.

Abstract

Objective: Cone beam CT (CBCT) images contain more scatter than a conventional CT image and therefore provide inaccurate Hounsfield units (HU). Consequently CBCT images cannot be used directly for dose calculation. The aim of this study is to enable dose calculations to be performed with the use of cone-beam CT images taken during radiotherapy and potentially avoid the necessity of re-planning.

Methodology: A phantom and prostate cancer patient with a metallic prosthetic hip replacement were imaged using both CT and CBCT. The multilevel threshold algorithm (MLT) was used to categorise pixel values in the CBCT images into segments of homogeneous HU. The variation in HU with position in the CBCT images was taken into consideration and the benefit of using a larger number of materials than typically used in previous work has been explored. This segmentation method relies upon the operator dividing the CBCT data into a set of volumes where the variation in the relationship between pixel values and HUs is small. A field-in-field (FIF) treatment plan was generated from the CT of the phantom. An intensity modulated radiation therapy (IMRT) plan was generated from CT images of the patient. These plans were then copied to the segmented CBCT data sets with identical settings and the doses were recalculated and compared.

Results: In the phantom study, gamma evaluation showed that the percentage of points falling in planning target volume (PTV), rectum and bladder with $\gamma < 1$ (3%/3 mm) was 100%. In the patient study, increasing the number of bins to define the material type from 7 materials to 8 materials, required 50% more operator time to improve the accuracy by 0.01% using pencil beam (PB) and collapsed cone (CC) and 0.05% when using Monte Carlo (MC) algorithms.

Conclusion: The segmentation of CBCT images using the method in this study can be used for dose calculation. For a simple phantom, two values of HU were needed to improve dose calculation accuracy. In challenging circumstances such as that of a prostate patient with hip prosthesis, five values of HU were found to be needed, giving a reasonable balance between dose accuracy and operator time.

KEYWORDS: CBCT-based dose calcualtion; ART; multilevel threshold algorithm; MC dose calculation.

1 Introduction

During external beam radiotherapy (EBRT) of the prostate, interfractional motion occurs due to changes in patient shape, patient positioning and internal organ motion, making the daily delivery of a uniform radiation dose to the treatment volume challenging (1). Interfractional motions such as variations in bladder and rectum volume have been demonstrated to have significant effects on prostate position and a negative impact on the accuracy of the treatment course (2).

The implementation of image guided radiation therapy (IGRT) in clinical practice, such as kilovoltage cone beam computed tomography (kV-CBCT) which is integrated in linear accelerators, allows the possibility of imaging the patient in the treatment position, either before or after each treatment in 3D with sufficient soft tissue contrast (3).

Despite the image quality improvements, cone beam computed tomography (CBCT) still has more scatter compared to a conventional CT (fan beam), due to its cone-beam geometry, and this scatter depends on the scanned object size and collimator and filter used (4). In addition, limited gantry rotation speed and large field-of-view (FOV) in a single rotation worsen image quality. The image quality also depends on acquisition parameters, i.e. mA, kV and the number of projections. Therefore, CBCT images provide inaccurate Hounsfield units (HU) and, consequently, cannot be used directly for dose calculation. This means that currently, acquiring a new '*planning*' CT scan is necessary for accurate assessment of dose differences which is resource intensive and time-consuming, involving re-outlining structures in the new scan and copying the original plan onto the new scan to obtain dose-volume histogram (DVH) information, thus additional dose to patient is delivered. Many papers have studied the use of CBCT data for dose recalculation, which is still an active area for research (5). The majority of these studies deal with adjustment techniques to correct CBCT HU values, such as mapping the HUs in CT images to the equivalent points in the CBCT image geometry after rigid registration (6-8). In addition, image cumulative histograms can be used to adjust HU values between planning CT (pCT) and CBCT images (5,6). Another technique uses a multilevel-threshold (MLT) algorithm as proposed by Boggula et al (2007), where the pixel values of CBCT images were replaced with a small number of fixed HU values as in CT for air, soft-tissue and bone (9-11). In addition, Fotina et al. (2008) used the same technique, calling it a density override technique, but with a range of HU values for bone (soft bony structures, hard bone and teeth) and air/low density regions (rectal balloon

and lung). All other regions are assumed to be water-equivalent assigned with one HU value (5). In this work, the MLT algorithm has been used to categorise pixel values into segments on a region-by-region basis and the region size changes depending on the anatomical features. Thus the considerations of the variation in HU with position in the CBCT have been taken into account. Furthermore the benefit of a larger number of materials has been explored.

Further novelty in this study is the use of Monte Carlo (MC) modelling, in order to separate uncertainties in the dose calculation inherent in the treatment planning system, including those due to the influence of the Titanium implant, from uncertainties introduced by the threshold method.

2 Method and materials

2.1 *CBCT image acquisition*

The X-ray volumetric imaging integrated in an Elekta Synergy linear accelerator (XVI^{TM}, version 4.5, Elekta, Crawley, West Sussex, UK) was used to acquire CBCT images. The CBCT scans were acquired with a field of view (medium FOV) of 41 cm in diameter and 20.5 cm in the axial direction with a bowtie filter added (F1). The images were then transferred to the Oncentra MasterPlan (OMP) treatment planning system (version 4.3 Elekta, Netherlands) via DICOM protocol for dose calculation.

2.2 *Treatment planning system and planning CT*

2.2.1 Anthropomorphic phantom study

A male pelvis phantom was built using the Multiblock phantom that was designed by Seaby et al (12). The blocks length is 30 cm with a square or right angle triangle cross-section with sides of 4 cm. The blocks are made of two materials; WT1 for water (tissue equivalent) and IB7 for bone as shown in Figure 1. The pCT images of the phantom were acquired using a Philips Brilliance Big Bore CT scanner (Philips Medical Systems, version 2.3, Cleveland, Ohio, USA). Structures were drawn in the pCT to represent PTV, rectum and bladder. A field-in-field (FIF) plan with six 6-MV photon fields, at gantry angles of 0°, 90° and 270° was performed using the OMP. The prescription dose was 74 Gy in 37 fractions. The OMP supports two types of algorithm to

calculate dose distribution; collapsed cone (CC) and pencil beam (PB) algorithms, both were used in this study for dose calculations.

2.2.2 Patient study

This study was performed on a prostate cancer patient with a metallic prosthetic right hip replacement treated at the Department of Clinical Oncology and Radiotherapy, ABM University Health Board, Swansea, Wales. This case provides a good assessment of dose calculation using CBCT due to the difficulties presented by the metal artefacts in both pCT and CBCT images (see 2.3 section). The artefacts in pCT were reassigned as water in the original patient plan using a bulk density correction. An intensity modulated radiotherapy (IMRT) plan with five 6-MV photon fields, at gantry angles of 65°, 110°, 180°, 225°, and 325° was performed. The prescription dose was 74 Gy in 37 fractions. Dose distribution was calculated using PB and CC algorithms.

2.3 *Modification of CBCT images*

Since the CBCT images contain more scatter than a conventional CT system, the CBCT HU to electron density (ED) calibration used for dose calculation is more complex, as it can vary with position and with the presence of metallic implants. The MLT algorithm involves categorising pixel values in the CBCT images into segments of homogeneous HU using MATLAB scripts (Mathworks, Natick, MA) to generate segmented CBCT (sCBCT) data. For the phantom case, only two bins, where a bin is a region of a uniform HU value, were considered (sCBCT2) that represent water and hard bone. For the patient case, there is a range of soft tissue types and different materials densities, thus more bins are needed to take into account this variation. Therefore, the maximum number of bins used in this study was eight bins, sCBCT8, that represent air (-976 HU), two adipose tissues (-135 & - 96 HU), water (0 HU), muscle (48 HU), soft bone (200 HU), hard bone (600 HU) and metal implants (2976 HU) (see Table 1). Then the soft bone bin was excluded and considered as hard bone in sCBCT7 and sCBCT6 excluded the muscle bin and considered it as water. In sCBCT5, the adipose1 bin was excluded and considered as adipose2 while sCBCT4 excluded both adipose bins. The minimum number of bins used was three bins, sCBCT3, that represent air, water and hard bone, which are the main materials in the pelvis region. The combination of different bins in each sCBCT was chosen to create a realistic balance between the main three materials. The range of pixel values in the CBCT images were: air (0

to 200), adipose tissue (201 to 600 & 601 to 700), water (701 to 800), muscle (801 to 875), soft bone (876 to 1000), hard bone (1001 to 1600) and metal implant (1601 to 8000).

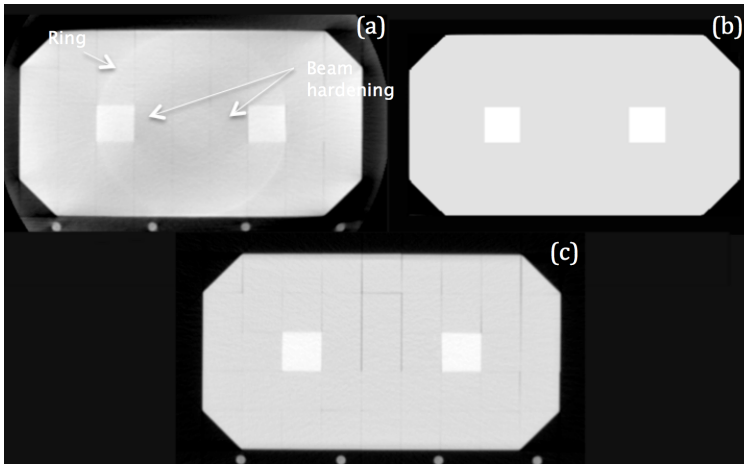

Fig. 1: Multiblock phantom scan using (a) CBCT and (c) pCT and the resultant image after segmenting CBCT (b).

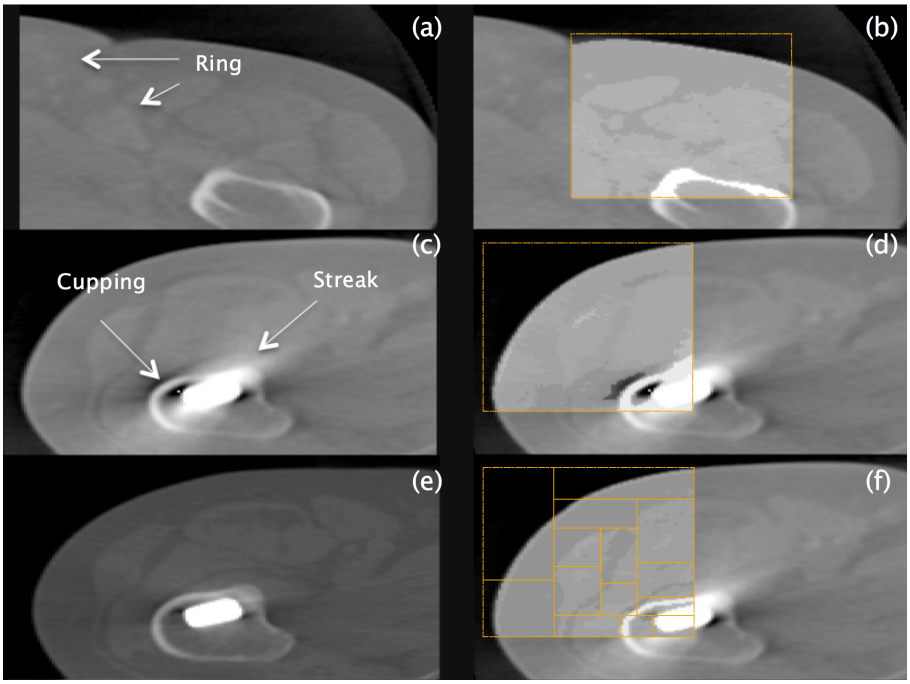

Fig. 2: Two different locations and slices of the original CBCT (a and c) and the resultant images after segmentation using the same threshold values in only a part of the image (b and d respectively). In particular it is observed in (d) that the artefacts in the vicinity of the metal are erroneously corrected. Variable threshold values were then used (f) which compared well with the original pCT image (e).

The phantom materials are uniform and thus the effect of scatter in CBCT can be observed. However, one set of threshold values for each material of these intervals were broad enough to correct for scatter as well as ring artefacts, which occur due to uncorrected variations in detector defects and linearity. The method also corrected beam hardening artefacts that result in shading artefacts throughout the centre of the phantom as shown in Figure 1. For the patient case, the threshold values change geometrically since noise and scatter in CBCT is variable, dependent

on position in the image especially in the presence of high density materials (13). Figure 2(a and c) shows two different slices and different locations of the original CBCT images. Figure 2(b) shows the segmentation of the pixel values using specific threshold values, which can correct ring artefacts. These values are valid even in high density regions. On the other hand, in the presence of the hip prosthesis (higher density region), these threshold values are no longer valid and would overestimate the HU values around that region due to the increased amount of X-ray scatter and beam hardening resulting in two forms of artefact, cupping or dark shading, and streaks as shown in Figure 2(d). The artefacts affect the pixel values and therefore affect the segmentation compared with the pCT image (Fig. 2e). This means that the CBCT data should be divided into regions with sets of different threshold values, which are determined on a region-by-region basis, and should be applied to these regions to accurately correct for the artefacts, as shown in Figure 2(f). In general, the greater the variation in the scatter the greater the number of regions that need to be considered and the size of the region decreases as it gets closer to inhomogeneities. Thus, threshold values were highly variable across the whole CBCT data set in this study, particularly in the presence of the hip prosthesis.

2.4 *Monte Carlo calculation*

The Elekta Synergy linear accelerator was modeled using Electron Gamma Shower (EGSnrc), which is one of the most popular Monte Carlo (MC) codes for medical physics (14). BEAMnrc and DOSXYZnrc are two applications in EGSnrc code that are used to simulate the beam generated from the treatment head and to score dose deposition in voxel grids, respectively. In this study, 90 million particles were used for each beam to provide an accurate simulation with a low statistical uncertainty. High performance computing (HPC-Wales) was used to speed up MC calculations (15). The MC normalization was performed by calculating the dose in a water

Table 1: Number of bins used in sCBCT.

	Material							
Bins	Air	Adipose1	Adipose2	Water	Muscle	Soft bone	Hard bone	Titanium alloy
sCBCT3	✔	✗	✗	✔	✗	✗	✔	✗
sCBCT4	✔	✗	✗	✔	✗	✗	✔	✔
sCBCT5	✔	✗	✔	✔	✗	✗	✔	✔
sCBCT6	✔	✔	✔	✔	✗	✗	✔	✔
sCBCT7	✔	✔	✔	✔	✔	✗	✔	✔
sCBCT8	✔	✔	✔	✔	✔	✔	✔	✔

phantom under the standard reference conditions (10 × 10 field size, 100 cm source-to-surface distance, 5 cm depth).

2.5 *Treatment planning evaluation and comparison*

The sCBCT and pCT images were fused using ProSoma software (v3.3, MedCom, Germany) and the structure sets were then transferred to the sCBCT images without any modification except the external contour for the patient case where there are some differences. The plans were then copied to sCBCT using the same geometry and MU values and doses were recalculated using PB and CC algorithms. For MC calculation, the pCT artefacts were changed to a water material of uniform density using a MATLAB script. The MC dose calculation was then performed on pCT and sCBCT images using the same HU-ED calibration as in OMP (Fig. 3). The MC dose file (.3ddose) and the DICOM-RT file were then imported into the computational environment for radiotherapy research (CERR) software to compare the resultant dose distribution (16). For both studies, dose volume histogram (DVH) were compared between pCT and sCBCT plans. The maximum dose (D_{max}), mean dose (D_{mean}) and minimum dose (D_{min}) parameters for PTV, rectum and bladder were compared. To quantitatively appraise the differences between pCT and sCBCT plans, especially for the PTV, rectum and bladder, a gamma index analysis was performed using the pCT plan as a reference. The criteria were set as 3 mm distance to agreement (DTA) and 3% dose difference (DD) and 5% low dose threshold (17). For the patient study only, the cross-plane profiles of pCT, sCBCT3 and sCBCT8 plans at the isocentre depth were compared and the conformity index (CI) was calculated for all sCBCT plans and then compared with the pCT plans using PB, CC and MC algorithms (18). In addition, the dose at the isocentre (at the geometric centre of the prostate PTV (PTVp)) was compared between the pCT and sCBCT plans and plotted against the operator time required for defining the threshold values for different regions. The more the variation of scatter the more regions need to be defined. Thus the operator time increases as the number of anatomical materials involved increases.

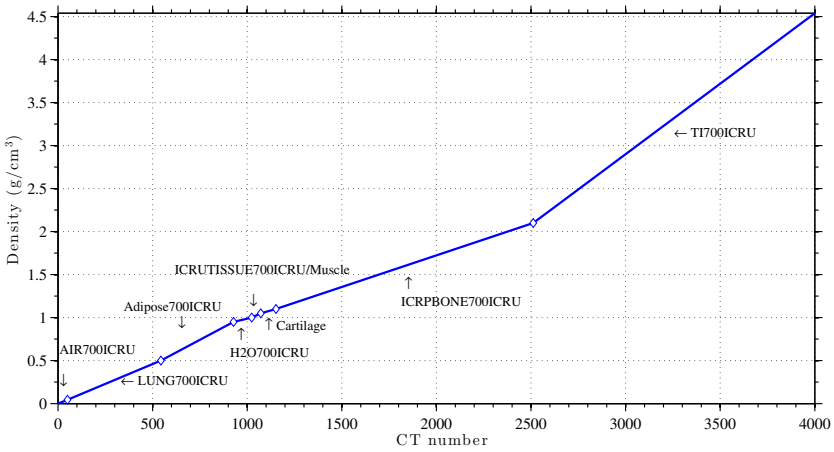

Fig. 3: The CT ramp for the conversion of CT values to material type and densities used in OMP. The same ramp was used in MC, the density and composition of the material used in this ramp were included in the PEGS4 cross section data file.

3 Results and discussion

3.1 Phantom study

Figure 4 shows the DVH of a prostate FIF plan with a prescription dose of 74 Gy in 37 fractions. The sCBCT2 plan showed a good agreement with the pCT plan. In terms of PTV coverage, the dose difference in D_{mean} between the pCT and sCBCT2 plans was 0.16 % when using MC algorithm and the dose difference in D_{max} was -0.25 % and in D_{min} was 1.1 % (see Table 1 in the Appendix 1 for PB and CC algorithm).

Figure 5 shows dose difference in D_{mean} between pCT and sCBCT2 using PB, CC and MC algorithms. For PTV, the difference in D_{mean} between pCT and sCBCT2 plans was 0.01%, 0.06% and 0.1% using PB, CC and MC algorithm respectively. The largest difference between pCT and sCBCT2 plans was for the bladder mean dose which was overestimated by sCBCT

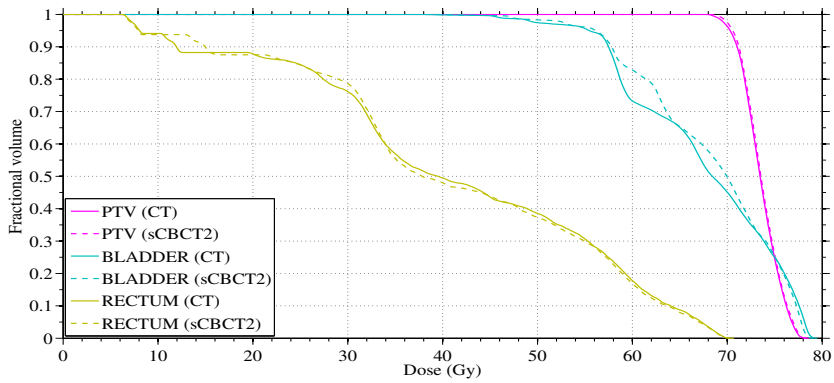

Fig. 4: DVHs comparison between pCT (solid line) and sCBCT2 (–) FIF plans for PTV, rectum and bladder using MC algorithm (prescription dose 74 Gy).

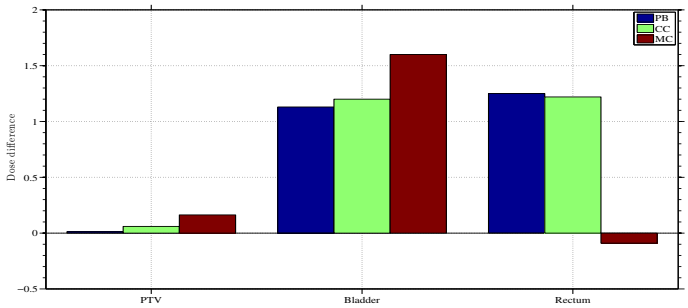

Fig. 5: Dose differences in mean dose between pCT and sCBCT2 for PTV, bladder and rectum using PB, CC and MC algorithms.

plan by 1.13%, 1.2% and 1.6% using PB, CC and MC algorithm respectively. Gamma evaluation showed that the percentage of points in the PTV, rectum and bladder with $\gamma < 1$ (3%/3 mm) was 100% using all algorithms showing that two bins were enough to improve the dose accuracy for such a simple phantom.

3.2 Patient study

Figure 6 shows the cross-plane profile/x profile of pCT, sCBCT8 and sCBCT3 at the depth of the plan isocentre as well as the CT number of the pCT scan at that depth. Only sCBCT3 and sCBCT8 profiles were plotted to show the clear improvement in the match with the pCT profile when increasing from 3 to 8 values of HU. It can be seen that the sCBCT8 profile is in good agreement with the pCT profile compared with the sCBCT3 profile. The largest difference between the pCT and sCBCT8 plans was at the implant/tissue interface where sCBCT8 was 25.9 Gy and pCT was 29.1 Gy. This is due to the fact that the HUs in this region were affected by artefacts due to the presence of the metal. These artefacts were reassigned as water in the original patient plan using a bulk density correction, whereas sCBCT8 was segmented based on the actual HUs of pCT. On the other hand, the sCBCT3 profile overestimated the dose across the metal up to 3.96 Gy (50%). This is due to the fact that the sCBCT3 approach does not include the HU of metal and thus considers that region as hard bone.

Figure 7 shows the DVH of a prostate IMRT plan with a prescription dose of 74 Gy. It shows the dose of sCBCT8, sCBCT5, sCBCT3 and pCT plans to the 95% volume of the PTV, rectum and bladder using the CC algorithm.

In terms of PTV coverage, the lowest difference between the pCT and sCBCT plans was achieved by the sCBCT8 plan while the largest difference was obtained by the sCBCT3 plan, which provided less anatomical materials compared with sCBCT8. The results showed that

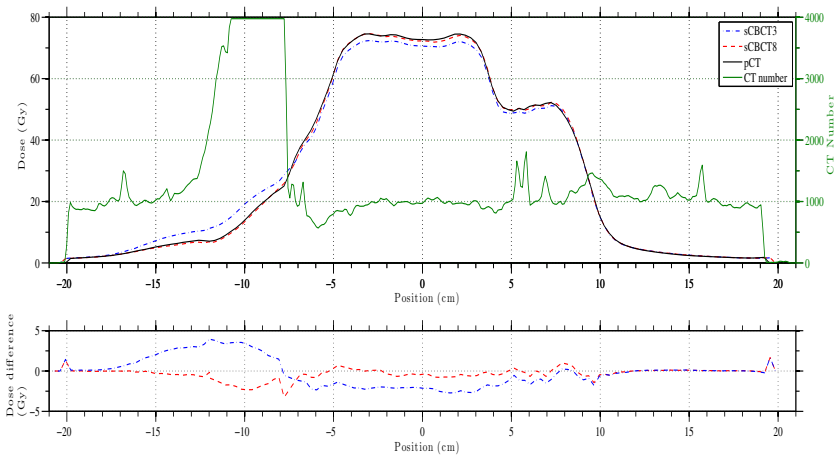

Fig. 6: Comparison of the dose profile of pCT, sCBCT3 and sCBCT8 plans at the isocentre depth and the difference between sCBCT3/sCBCT8 and pCT using CC algorithm.

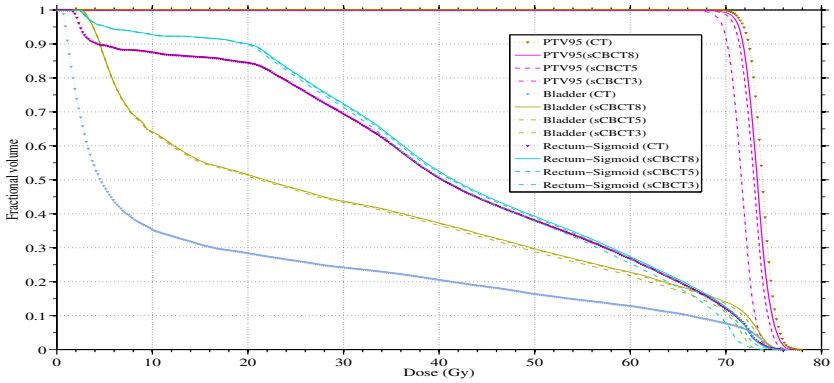

Fig. 7: DVHs comparison pCT (:v), sCBCT8 (solid line), sCBCT5 (–) and sCBCT3 (-.) IMRT plans for PTV95, rectum and bladder using CC algorithm.

the differences between CT and sCBCT increased as the number of bins decreased (see Table 2 in the Appendix 1). It is worth mentioning that there are some differences in the bladder and rectal volume between the pCT and CBCT scans. The bladder volume, for example, is significantly reduced in the CBCT scan ($> 25\%$ reduction). Therefore, the differences are not directly comparable indicting that deformable image registration (DIR) was needed rather than rigid image registration to correct for organ deformation between pCT and CBCT. Currently, only rigid image registration is available for clinical use. In addition, deforming the pCT to match the CBCT anatomy so that the original HU are copied onto the CBCT could be used as a benchmark for the study. Yang et al (2007) used deformable electron density mapping on CBCT images and reported that the dose difference between pCT and CBCT was within 2% in three prostate patients (7). More recently, Onozato et al (2014) used the MLT algorithm as well as DIR on CBCT images of ten prostate patients and achieved better accuracy ($< 1\%$) (11). For some patients, the accuracy was not improved mainly due to the large artefacts from gold fiducial markers and bowel gas in CBCT images, which could have been corrected if the threshold values

were changeable geometrically. None of these studies used a patient with prosthesis.

Figure 8(a) shows the γ agreement index (γAI) for the calculation points falling inside the PTV, rectum and bladder for different bins, showing the fraction of points resulting with $\gamma < 1$. In general, as the number of bins decreased the number of calculation points which passed ($\gamma < 1$) decreased slightly at first and then significantly when moving from 5 to 4 bins for all algorithms. The number of points that passed remained almost unchanged when going from 4 to 3 bins except for the rectum region where it dropped from 0.68% to 0.22% when using PB and from 2% to 1.8% when using CC algorithm. For the PTV and bladder region, all the calculation points passed the gamma test for 5 up to 8 bins when using the PB algorithm, while using the CC algorithm, 0.89% showed $\gamma > 1$ for the PTV, and 1.5% for the bladder, when using the same bins. When using MC, the number of calculation points that showed $\gamma < 1$ decreased almost linearly as the number of bins decreased. It is worth mentioning that the PB algorithm in OMP calculates dose to water while, the CC algorithm calculates dose to medium as does the MC algorithm (19). Since MC and CC algorithms calculate dose to medium, the HU of the medium must be provided precisely. Therefore, the PB algorithm would be less sensitive than CC and MC for calculating the dose using different bins as shown in Figure 8. Thus MC and CC algorithms minimised uncertainty related to the dose calculation as well as identifying those introduced by different bins.

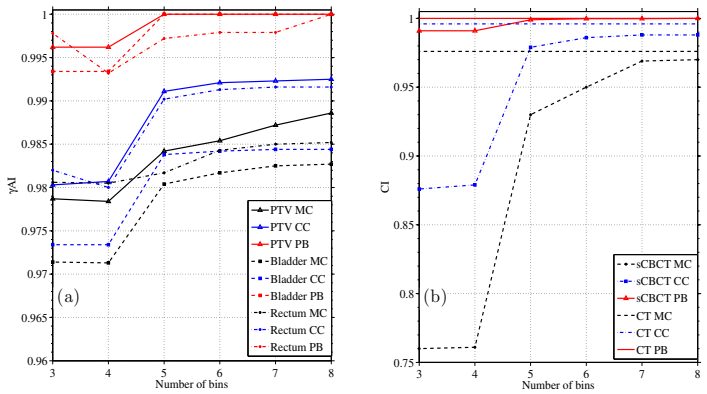

Fig. 8: (a) Summary of the γ index with fixed DTA = 3 mm and DD = 3% for the calculation points falling inside the PTV, rectum and bladder, showing the fraction of points resulting with $\gamma < 1$. (b) Conformity index (CI)comparison between pCT and sCBCT plans using PB, CC and MC algorithms against number of bins.

Figure 8(b) shows the CI values of the sCBCT plans and the difference compared with pCT using PB, CC and MC algorithms. In the figure the three horizontal lines indicate the CI value of the pCT plan using PB, CC and MC algorithm. The CI value was almost consistent when going

from the sCBCT8 to the sCBCT7 plan using all algorithms. The most significant change in the CI value was found when moving from the sCBCT5 plan to the sCBCT4 plan, going from 0.979 to 0.879 when using the CC algorithm and from 0.93 to 0.761 when using the MC algorithm. As a result, it showed that going for less than 5 bins for such a case would cause a difference of at least 15% in the CI values compared with pCT.

Figure 9 shows the dose difference between pCT and sCBCT plans at the isocentre using all algorithms plotted against the operator time needed to segment each sCBCT bin. The sCBCT5 to sCBCT8 plans showed differences of less than -2% compared with the pCT plan when using the PB and CC algorithms, which is considered to be clinically acceptable. For the MC algorithm, only the sCBCT7 and sCBCT8 plans showed similar differences. It can be clearly seen that as the number of bins increased the operator time increased as shown in Figure 9. From sCBCT7 to sCBCT8, it required 50% more operator time to improve the accuracy by 0.01% when PB and CC algorithms were used for dose calculation and 0.05% when using MC algorithm. It required about 55% less time to improve the accuracy by 1.13%, 1.26% and 1.45% using PB, CC and MC algorithms respectively. Therefore, the 5 bins is the optimal level which balances between the accuracy of the calculation and the time required. This time would be greatly reduced with automation, which is currently being investigated, but there is likely to be a certain amount of operator intervention and the relative amount of operator time is likely to be dependent on the number of bin chosen. Furthermore, work has been begun to examine a patient with bilateral metal hip prostheses, where the operator time would be expected to be longer.

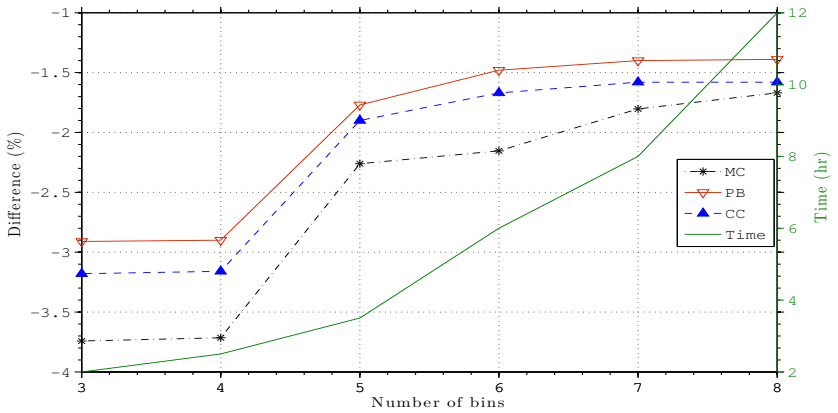

Fig. 9: Dose comparison between pCT and sCBCT plans at the isocentre against operator time using PB (..), CC (–) and MC (-.) algorithms.

4 Conclusion

The segmentation of CBCT images using the method in this study can be used for dose calculation. For a simple phantom, the result showed that two values of HU would be enough to provide a good dose accuracy. For a prostate patient with hip prosthesis, the optimal level of operator effort that balances between dose accuracy and calculation time was found when only five values of HU, which include air, adipose, water, hard bone and metal implant HU values, was used. Thus this method is feasible for adaptive radiotherapy (ART), as an alternative to obtaining a new planning CT and re-outlining the structures, which can take up to a day in a busy radiotherapy department.

Reference

1. Langen KM, Jones DTL. Organ motion and its management. International Journal of Radiation Oncology* Biology* Physics. 2001;50(1):265-78.

2. Ciernik IF, Baumert BG, Egli P, Glanzmann C, Ltolf UM. On-line correction of beam portals in the treatment of prostate cancer using an endorectal balloon device. Radiotherapy and oncology. 2002;65(1):39-45.

3. Jaffray DA, Siewerdsen JH, Wong JW, Martinez AA. Flat-panel cone-beam computed tomography for image-guided radiation therapy. International Journal of Radiation Oncology* Biology* Physics. 2002;53(5):1337-49.

4. Stock M, Pasler M, Birkfellner W, Homolka P, Poetter R, Georg D. Image quality and stability of image-guided radiotherapy (IGRT) devices: A comparative study. Radiotherapy and Oncology. 2009;93(1):1-7.

5. Fotina I, Hopfgartner J, Stock M, Steininger T, Ltgendorf-Caucig C, Georg D. Feasibility of CBCT-based dose calculation: comparative analysis of HU adjustment techniques. Radiotherapy and Oncology. 2012;104(2):249-56.

6. van Zijtveld M, Dirkx M, Heijmen B. Correction of conebeam CT values using a planning CT for derivation of the dose of the day. Radiotherapy and Oncology. 2007;85(2):195-200.

7. Yang Y, Schreibmann E, Li T, Wang C, Xing L. Evaluation of on-board kV cone beam CT (CBCT)-based dose calculation. Physics in medicine and biology. 2007;52(3):685-705.

8. Richter A, Hu Q, Steglich D, Baier K, Wilbert J, Guckenberger M, et al. Investigation of the usability of conebeam CT data sets for dose calculation. Radiat Oncol. 2008;3(1):42.

9. Boggula R, Wertz H, Lorenz F, Madyan YA, Boda-Heggemann J, Schneider F, et al. A proposed strategy to implement CBCT images for replanning and dose calculations. International Journal of Radiation Oncology* Biology* Physics. 2007;69(3):S655-S6.

10. Boggula R, Lorenz F, Abo-Madyan Y, Lohr F, Wolff D, Boda-Heggemann J, et al. A new strategy for online adaptive prostate radiotherapy based on cone-beam CT. Zeitschrift fr Medizinische Physik. 2009;19(4):264-76.

11. Onozato Y, Kadoya N, Fujita Y, Arai K, Dobashi S, Takeda K, et al. Evaluation of On-Board kV Cone Beam Computed TomographyBased Dose Calculation With Deformable Image Registration Using Hounsfield Unit Modifications. International Journal of Radiation Oncology*

Biology* Physics. 2014;89(2):416-23.

12. Seaby AW, Thomas DW, Ryde SJS, Ley GR, Holmes D. Design of a multiblock phantom for radiotherapy dosimetry applications. The British journal of radiology. 2002;75(889):56-8.

13. Pineda AR, Siewerdsen JH, Tward DJ, (eds). Analysis of image noise in 3D cone-beam CT: Spatial and Fourier domain approaches under conditions of varying stationarity. P Proc SPIE 2008; 6913:69131Q-69131Q-10.

14. Kawrakow I, Rogers DWO. The EGSnrc code system. NRC Report PIRS-701, NRC, Ottawa. 2000.

15. HPC Wales. Wales, UK. http://www.hpcwales.co.uk/. Accessed 08 December 15.

16. Deasy JO, Blanco AI, Clark VH. CERR: a computational environment for radiotherapy research. Medical physics. 2003;30(5):979-85.

17. Nelms BE, Simon JA. A survey on IMRT QA analysis. Journal of applied clinical medical physics. 2007;8(3):76-90.

18. ICRU. International Commission on Radiation Units and Measurements. Prescribing I. recording, and reporting photon-beam intensity-modulated radiation therapy (IMRT). ICRU Report 83. J ICRU. 2010;10:1-106.

19. Knöös T, Wieslander E, Cozzi L, Brink C, Fogliata A, Albers D, et al. Comparison of dose calculation algorithms for treatment planning in external photon beam therapy for clinical situations. Physics in medicine and biology. 2006;51(22):5785.

List of Figures

Appendix 1

Table. 1: Dose and coverage differences between sCBCT2 plan and pCT plan in % for the PTV, rectum and bladder using PB, CC and MC algorithms for the phantom case

SCAN		sCBCT2		
		PB	CC	MC
PTV	Dmax	0	0.25	-0.25
	Dmean	0.01	0.06	0.16
	Dmin	0.28	0.29	1.19
Rectum	Dmax	-0.56	-0.28	-0.56
	Dmean	1.24	1.25	-0.09
	Dmin	26.08	19.71	3.17
Bladder	Dmax	-0.24	-0.75	0
	Dmean	1.13	1.22	1.63
	Dmin	0.49	1.99	1.61

Table. 2: Dose and coverage differences between sCBCT plans and pCT plan in % for the PTV, rectum and bladder using PB, CC and MC algorithms for the patient case

SCAN		sCBCT8			sCBCT7			sCBCT6			sCBCT5			sCBCT4			sCBCT3		
		PB	CC	MC	PB	CC	MC	PB	CC	MC	PB	CC	MC	PB	CC	MC	PB	CC	MC
PTV	Dmax	-1.51	-1.02	-1.5	-1.51	-1.02	-1.5	-1.76	-1.02	-1.75	-2.01	-1.79	-2	-3.02	-2.82	-2.25	-3.02	-2.82	-2.25
	Dmean	-0.75	-0.695	-0.61	-0.76	-0.7	-0.68	-0.88	-0.8	-0.82	-1.33	-1.22	-1.1	-2.77	-2.93	-3.15	-2.77	-2.96	-3.15
	Dmin	-1.41	-5.19	-0.18	-1.41	-5.19	-1.9	-1.41	-5.48	-2.23	-2.26	-5.77	-2.61	-3.68	-6.92	-4.85	-3.68	-6.92	-4.85
Rectum	Dmax	-0.51	0.26	-1.27	-0.51	0.26	-1.28	-0.51	0.26	-1.28	-1.29	-0.52	-2.04	-2.58	-2.1	-4.59	-2.58	-2.1	-4.85
	Dmean	4.57	4.68	1.64	4.57	4.68	1.89	4.5	4.62	2.43	40	3.99	1.79	2.38	2.15	0.29	2.43	2.18	0.36
	Dmin	58.8	66.6	40	58.8	66.6	40	58.8	66.6	40	58.8	66.6	40	58.8	66.6	40	58.8	66.6	53
Bladder	Dmax	-0.77	-0.52	-0.78	-0.077	-0.52	-0.76	-0.77	-0.52	-0.76	-1.28	-1.3	-1.3	-3.08	-3.39	-2.87	-3.08	-3.39	-3.13
	Dmean	72.34	71.03	63.28	72.33	71.02	63.24	72.15	70.9	63	71.31	70.1	62.2	68.84	67.08	59.6	68.91	67.02	59.7
	Dmin	285	97.83	171.4	285	257	171.4	285	257	171.4	285	257	171.4	285	285	171.4	285	285	171.4